

Attosecond science in atomic, molecular, and condensed matter physics

Stephen R. Leone^{abc} and Daniel M. Neumark^{*ac}

Received 29th July 2016, Accepted 16th August 2016

DOI: 10.1039/c6fd00174b

Attosecond science represents a new frontier in atomic, molecular, and condensed matter physics, enabling one to probe the exceedingly fast dynamics associated with purely electronic dynamics in a wide range of systems. This paper presents a brief discussion of the technology required to generate attosecond light pulses and gives representative examples of attosecond science carried out in several laboratories. Attosecond transient absorption, a very powerful method in attosecond science, is then reviewed and several examples of gas phase and condensed phase experiments that have been carried out in the Leone/Neumark laboratories are described.

Introduction

Physical chemistry has benefited tremendously over the last several decades by the evolution of time-resolved experimental techniques. Advances up to the year 2000 were elegantly described in a review article by Zewail,¹ which discusses how our ability to understand fundamental chemical processes is inextricably linked to the development of methods ranging from flash photolysis to femtosecond lasers. It is now almost routine (albeit expensive!) in chemical physics laboratories to perform experiments that follow detailed and complex molecular motions in real time, using femtosecond lasers that can monitor rotational and vibrational motion, dissociation on bound and repulsive potential energy surfaces, and passage through conical intersections and over transition states. Experiments based on femtosecond methodology can in principle track even the highest frequency vibrations, such as the 7.5 fs vibrational period of the H–H fundamental in H₂.

The next frontier in time-resolved chemical dynamics is the study of electronic dynamics.^{2,3} While femtosecond experiments often explore the effects of electron dynamics on nuclear motion, following the electrons themselves requires the development of light sources offering attosecond (as) time resolution; as an example, the classical period of an electron in its ground state orbiting the

^aDepartment of Chemistry, University of California, Berkeley, CA 94720, USA. E-mail: dneumark@berkeley.edu

^bDepartment of Physics, University of California, Berkeley, CA 94720, USA

^cChemical Sciences Division, Lawrence Berkeley National Laboratory, Berkeley, CA 94720, USA

hydrogen atom is ~ 150 as. Since 2000, developments in laser technology, optics, and atomic and molecular physics have made it possible to generate isolated attosecond pulses as short as 67 as.⁴ These technical advances have enabled efforts in many laboratories throughout the world to perform attosecond science experiments that reveal new dynamical time scales in atoms, molecules, liquids, and solids, as discussed in numerous recent reviews.^{5–16} This article provides a brief overview of key developments in attosecond science and technology, followed by a discussion of examples that have been carried out in our laboratories at Berkeley over the last several years.¹⁶

Generation and characterization of attosecond light pulses

Commercial femtosecond laser systems typically employ Ti:sapphire crystals as the active medium. They operate at a central wavelength of around 800 nm, and high power systems involving either multipass or regenerative amplifiers can generate pulses as short as 20 fs. Using a combination of self-phase modulation in optical fibers to increase the bandwidth of the pulse and chirped mirrors to temporally compress the spectrally broadened pulse, one can obtain “few-cycle” near-infrared (NIR) pulses with pulse durations as short as 3–5 fs. The optical period of 2.6 fs for an 800 nm pulse places a lower bound on the pulse duration attainable at this wavelength. Very recently, pulses spanning the visible region of the spectrum with sub-fs peak electric fields have been synthesized.¹⁷ Nonetheless, generation of the shortest attosecond pulses generally requires upconversion to the vacuum ultraviolet/soft X-ray region where the optical period is substantially shorter (*i.e.* 41 as at 100 eV).

Owing to these considerations, attosecond pulse generation is strongly linked to the phenomenon of high harmonic generation (HHG).^{18–24} This process involves strong-field manipulation of electrons by focusing a femtosecond laser pulse to high intensities in a target material, typically inert gas in a cell, gas jet, or waveguide, and generates light pulses covering the extreme ultraviolet (XUV) and soft X-ray regime of the electromagnetic spectrum. HHG is typically interpreted using a three-step model.^{20,21} First, the high field intensities around the maximum of the electric field cycles of the focused driver pulse distort the electronic potential, resulting in tunneling ionization of the gas and the release of electron wave packets into the continuum. The ejected electrons are accelerated away and then toward the parent ion as the laser electric field changes sign, gaining energy from the field. Finally, the inelastic recollision of these accelerated electrons with the parent ion releases excess kinetic energy in brief attosecond light bursts each half-cycle of the driving field. The upper limit for the emitted energy, called the cut-off energy,^{20,22,25} is determined by the maximum amount of kinetic energy gained in the second step and is given by

$$E_{\max} = I_p + 3.17U_p, \quad (1)$$

where I_p is the ionization potential of the target gas, and U_p is the ponderomotive energy of the photoelectrons in the applied electric field, $U_p = E_{\text{laser}}^2/4\omega_{\text{laser}}^2$ (in atomic units).

Typical cut-off energies at 800 nm range from ~ 30 eV in Xe to >100 eV in Ne. HHG out to 1 keV has been observed in He but with a very low flux. At longer wavelengths, the ponderomotive energy is larger for the same laser intensity, resulting in a higher cut-off energy.²⁶ There has been considerable progress in recent years in experimentally realizing higher cut-off energies with longer wavelength driving pulses, with an important goal being to obtain useable intensities from HHG in the “water window” between 300 and 500 eV;^{27–34} this interval lies above the carbon K-edge but below the oxygen K-edge. Efficient HHG out to 280 eV has also been demonstrated recently using ultraviolet driving pulses.³⁵

In general, if a driving pulse comprising multiple optical cycles is used for HHG, then the temporal envelope of the HHG pulse is similar to that of the driving pulse. However, around the year 2000,^{36–38} it was realized theoretically and shown experimentally that under the right conditions, the HHG pulse comprises an attosecond pulse train with pulses occurring at twice the frequency of the driving field. The interference between these pulses yields a discrete harmonic spectrum comprising odd harmonics of the driving field up to the cut-off energy. Attosecond pulse trains have been used successfully in a series of elegant interferometry experiments that probe important features of electron dynamics.^{39–44} However, in many applications involving direct measurements of lifetimes and dynamics, isolated attosecond pulses are more desirable.

The generation of isolated attosecond pulses, first reported by the Krausz group in 2001,⁴⁵ required the development of novel advances in laser and optical technology, as well as new techniques for characterizing such pulses. These methods are generally based on isolating the XUV radiation produced by a single half-cycle of the driving field, or by suppressing XUV generation from all but a single half cycle. In amplitude gating,^{45,46} one combines appropriate energy filtering and carrier-envelope (C-E) phase stabilization of the driver pulse⁴⁷ to obtain an isolated attosecond pulse from a few-cycle driver pulse by reflecting (or transmitting) only the highest energy XUV radiation produced by the most intense half cycle of the driver pulse. This yields an isolated attosecond pulse comprising a continuous spectrum of photon energies close to the cut-off region. Amplitude gating has been used to generate pulses as short as 72 as centered at 105 eV, using Ne as the nonlinear medium.⁴⁸ The isolated attosecond pulses and the NIR pulses used to generate them are characterized by attosecond streaking,^{49,50} in which the

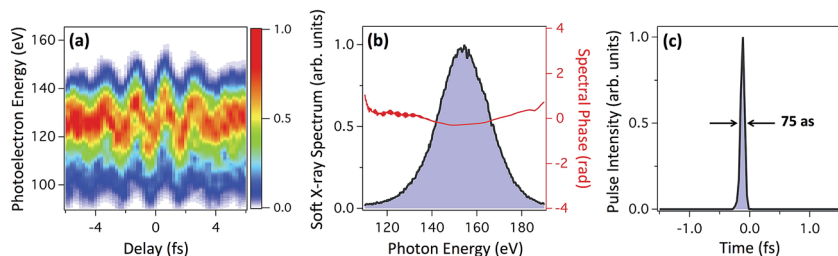


Fig. 1 Isolated attosecond pulse centered at 160 eV generated by amplitude gating. Panel (a) shows an attosecond streaking photoelectron spectrum, from which one extracts the spectral profile and phase (b) and the pulse duration (c).

momentum shifts by a C-E phase stabilized NIR pulse on the photoelectrons generated by the XUV pulse is determined as a function of delay between the two pulses. Fig. 1 shows an example of an isolated attosecond pulse centered at 160 eV along with its streaking trace and reconstruction, generated in our laboratory with amplitude gating using He as the gas medium.⁵¹

Amplitude gating requires exceedingly short (<4 fs) driver pulses and is thus quite technically demanding. Other gating methods have been developed in which isolated attosecond pulses can be generated from somewhat longer pulses and at lower XUV photon energies. These include polarization gating (PG),^{52,53} double optical gating (DOG),^{54–56} and ionization gating.^{57–59} PG and DOG rely on overlapping two counter-rotating circularly polarized pulses so that only a single half-cycle is linearly polarized and thus produces XUV light. In ionization gating, nearly isolated attosecond pulses are obtained by using ionization to terminate HHG after a particular half-cycle cut-off;⁶⁰ the central photon energy can be tuned by varying the C-E phase. A conceptually different method, the attosecond lighthouse, utilizes wavefront-rotated driver pulses to obtain high harmonic spectra consisting of spatially separated, isolated attosecond pulses.⁶¹ Our group has recently developed a gating scheme combining aspects of amplitude and polarization gating (PASSAGE, or Polarization ASSisted Amplitude GatE) that yields isolated attosecond pulses whose central frequency can be varied over energies ranging from 50–130 eV, and which can work with somewhat longer driving pulses than pure amplitude gating.⁶² Pulse energies from these methods are typically within an order of magnitude of one nJ. Several laboratories are aiming to generate μJ isolated attosecond pulses using very high power driving lasers,^{63,64} with the ultimate goal of performing attosecond pump–probe experiments (see later).

Representative examples of attosecond science

Time-resolved experiments using attosecond pulses offer superior time resolution combined with the capability to either initiate or probe dynamics in the soft X-ray region of the electromagnetic spectrum. Attosecond pulses in the range of 15–30 eV can probe Rydberg and high lying valence electronic states lying near or above the ionization potential of the target species. At higher energies, core ionization and core-to-valence transitions become accessible. The energies of these transitions are highly element-specific, enabling one to track the electronic dynamics associated with particular atoms in the gas phase and condensed phase targets. As technical advances push the useable cut-off energy of HHG to increasingly higher photon energies, more elements become accessible. As physical chemists, there is particular interest in reaching 300 eV, at which point transitions originating from the carbon K-edge become accessible. Recent reports indicate that this limit has in fact been reached.³³

On the other hand, intensities of isolated attosecond pulses achieved thus far are too low to routinely enable attosecond pump–probe experiments, which would truly take advantage of the time-resolution offered by these pulses. While pump–probe experiments using two attosecond pulse trains have been reported,^{39,65} as yet all dynamics experiments involving isolated attosecond pulses vary the time delay between an attosecond pulse and a much stronger, few-cycle NIR pulse. In many of these experiments, the temporal resolution is determined

by the cross correlation of the two pulses and thus corresponds to the intensity envelope of the NIR pulse, which can be as short as 3–5 fs. However, if the phase of the electric field of the NIR pulse relative to the attosecond pulse can be controlled, then one can observe dynamics associated with the NIR field and, in favorable cases, resolve dynamics on the attosecond time scale.

One of the first time-domain experiments using isolated attosecond pulses measured the lifetime of the 3d core hole in krypton created by an XUV pulse, which is filled by Auger recombination, emitting electrons from the 4p shell.⁶⁶ The lifetime of this process was determined using attosecond streaking, in which the emitted electrons interact with a few-cycle near-infrared pulse, and the evolution of the electron kinetic energy from the $M_{4,5}N_1N_{2,3}$ Auger line as a function of the relative delay between the two pulses reveals a 3d core hole lifetime of 7.9 fs.

Attosecond streaking has also been used to track the birth of photoelectrons in atoms and solids. In the first such experiment, an isolated sub-200-as pulse at 106 eV ionized neon atoms. Attosecond streaking yielded a delay of 21 ± 5 as in the photoemission of a 2s electron relative to a 2p electron in neon.⁶⁷ Theoretical efforts to understand the origin of this result have thus far underpredicted the measured value by approximately a factor of two.^{68,69} In a similar vein, attosecond photoelectron streaking spectroscopy was applied to study dynamics of electron escape from core and delocalized electronic states of a single crystalline tungsten $\langle 110 \rangle$ surface.⁷⁰ The experiment employed isolated XUV pulses with a pulse duration of ~ 300 as centered at 91 eV to simultaneously excite the 4f core level and the 5d and 6s conduction band electrons to upper conduction band states, leading to the creation of photoelectrons at the surface. The resulting attosecond streaking spectrogram yielded a delay of 110 ± 70 as for the emergence of 4f electrons relative to the conduction band electrons from the tungsten surface. More recently, attosecond streaking and coincidence techniques were combined to measure the difference in photoemission time delays between Ne and Ar, finding longer delays by up to 50 as in Ar that were attributed to resonance effects.⁷¹

Attosecond XUV pulses have been used to ionize a gas phase target that is then further ionized and/or dissociated by a few-cycle near-infrared pulse. Ions generated using this pulse sequence are detected by a time-of-flight spectrometer as a function of the time delay between the two pulses. This general type of experiment has been applied to systems ranging from inert gas atoms to polyatomic molecules. Electron tunneling ionization in neon was measured in real time using this technique.⁷² An attosecond pulse at 91 eV ejected a 2p electron and produced Ne^+ ions in several excited states ($2p^{-2}3p$, for example) *via* shake up. The Ne^{2+} yield was measured as a function of time-delay with respect to a NIR pulse. Steps in the Ne^{2+} yield in synchronicity with the electric field cycles of the NIR pulse were observed at delays near $\Delta t = 0$, where the most intense NIR field cycles overlap the XUV pulse. This step-like structure was attributed to field-induced tunneling of the $2p^{-2}3p$ and $2p^{-2}3s$ states. The ~ 380 as rise time for the steps was interpreted as an upper bound for the time to populate and tunnel from these states.

In a molecular application, an experiment combining isolated attosecond pulses, NIR excitation, and ion detection was performed to follow charge localization in H_2 and D_2 upon dissociative ionization.⁷³ This study measured the ultrafast charge redistribution of these molecules following dissociative

ionization to explore the coupling between electronic and nuclear motion on sub-femtosecond timescales. Here, an isolated attosecond XUV pulse ranging from 20 eV to 40 eV excited the molecule to doubly-excited electronic states that, left on their own, undergo dissociative ionization. The attosecond pulse was followed by a few-cycle near-infrared pulse that coupled the various neutral and ionic electronic states to one another as dissociation proceeded. The velocity and angular distributions of the resulting H^+ or D^+ photofragments were analyzed as a function of the delay between the two pulses. These experiments provide a sensitive measure of how the electron in dissociating H_2^+ or D_2^+ localizes onto a single atom *en route* to dissociation.

In a related experiment on a much more complex target, the phenylalanine molecule was ionized by an attosecond pulse covering 15–30 eV and then further ionized and fragmented by a few-cycle NIR pulse.⁷⁴ The yield of the immonium dication (R-CH-NH_2^{2+}) was measured as a function of pump–probe delay and found to oscillate with an average period of 4.3 fs. This time scale is considerably faster than the highest frequency X–H vibrations in the target. This difference in time scale was interpreted in terms of ultrafast hole migration to and from the NH_2 group in a superposition of excited cationic states created by the XUV pulse, an effect that had been predicted theoretically^{75–77} but not previously observed.

Finally, given the composition of this Faraday conference, it is appropriate to discuss how attosecond dynamics can be determined from high harmonic imaging/spectroscopy experiments. In 2004, Itatani *et al.*⁷⁸ demonstrated that by performing HHG experiments in laser-aligned molecules, one could analyze the spectrum of the high harmonics and obtain “tomographic images” of the Dyson molecular orbitals from which electric field induced ionization occurred. This very elegant method images electrons but is not explicitly time-resolved. Nonetheless, several laboratories^{79–83} have shown how one can extract attosecond dynamics from these experiments; two examples are summarized below.

In 2006, Baker *et al.*⁷⁹ performed an HHG experiment on H_2 , CH_4 , and their deuterated isotopologs in which an intense NIR pulse launches dynamics on an ionic potential energy surface. These dynamics evolve as the electron wavepacket, whose trajectory is controlled by the NIR laser field, recombines with the ion, producing high harmonic emission that is spectrally resolved using a diffraction grating. Ionization accesses the repulsive region on the H_2^+ potential energy curve, so the atoms separate during the electron trajectory. As a result, the higher harmonics, which are produced from longer-time trajectories (*i.e.* higher recombination energies), are depleted. To calibrate this effect in terms of molecular motion, HHG signals were compared for H_2 and D_2 ; the higher harmonics were indeed less depleted for D_2 . Hence, nuclear dynamics are resolved on the time scale of recombination, from 0.5 to 1.6 fs for an 800 nm pulse under the reported conditions. Similar experiments on CH_4 and CD_4 probed the initial complex vibrational dynamics that occur upon ionization to the Jahn–Teller-active ground state of CH_4^+ , whereupon the ion undergoes distortion from the initial tetrahedral geometry of the neutral.

More recently, high harmonic spectroscopy has been used to follow hole-migration dynamics in iodoacetylene (HCCI).⁸³ The HCCI molecules were impulsively aligned and then subjected to a few-cycle pulse at either 800 or 1300 nm with the target molecules aligned either perpendicular or parallel to the polarization of the newly created HHG pulse. The HHG driving pulse creates

a superposition of the X and A states of HCCl^+ , and the HHG spectrum upon recombination tracks the hole migration resulting from this superposition. In the perpendicular alignment configuration, the HHG pulse measures but does not affect the hole migration dynamics, *i.e.* the hole dynamics are “quasi-free”. Analysis at the two driving wavelengths shows that the hole is initially created on the I atom and oscillates to and from the C–C π molecular orbital with a period of 1.85 fs. The results for parallel alignment are strikingly different, illustrating that the HHG driving laser causes the tunneling electron to chase the charge migration dynamics in this configuration. For example, the population amplitudes of the X and A states in the perpendicular alignment are approximately equal, whereas in the parallel configuration at 800 nm, the population of the X state is significantly depleted at a recombination time of 1 fs. The difference in population amplitudes between these alignment configurations indicate that the HHG driving laser manipulates the A–X ionic transition, affecting both the amplitude and the relative phase of the two ionic states as the hole migration evolves.

Attosecond transient absorption

One of the most powerful methods in attosecond science is attosecond transient absorption (ATA) spectroscopy.^{84,85} In this section, experiments based on attosecond transient absorption and its variants are discussed, with particular emphasis on work that has been carried out at Berkeley. An example of an ATA apparatus⁸⁴ is shown in Fig. 2.

Here, an NIR pulse passes through a beamsplitter. The transmitted beam passes through optics appropriate for double optical gating and thus produces an isolated attosecond pulse in the HHG cell. The HHG output is focused by means of a toroidal mirror through the hole mirror (HM) into the sample, then dispersed by a grating onto an X-ray CCD camera. The reflected portion of the NIR beam passes through a variable delay stage and is combined with the XUV pulse *via* reflection by the hole mirror to overlap with the XUV beam at the sample. The metal filter downstream of the sample transmits the XUV beam but blocks the NIR beam. In an ATA experiment, one determines how the absorption spectrum of the broadband XUV pulse, as measured by the grating/camera combination, varies with the delay time between the XUV and NIR pulses. Remarkably, in ATA, one can obtain high resolution absorption spectra ($\sim 10\text{--}30$ meV, depending on the grating and central XUV photon energy) with no loss in temporal resolution. Hence, the broad bandwidth of the isolated attosecond pulse does not have any

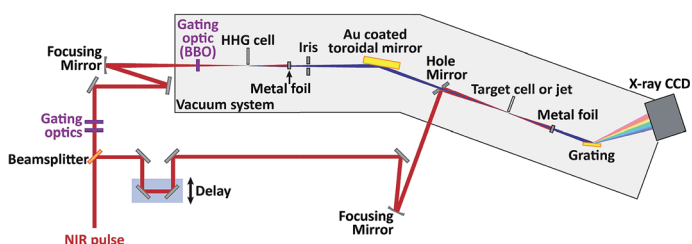


Fig. 2 Schematic of attosecond transient absorption experiment (adapted from ref. 84).

adverse consequences on the spectral resolution of the experiment. In fact, using such a pulse allows one to examine transient phenomena over a wide spectral range, resulting in a highly multiplexed experiment. These considerations make ATA an extremely powerful and versatile method in attosecond science.

ATA experiments can be performed with the NIR pulse preceding the XUV pulse, in which case the NIR and XUV pulses act as the pump and probe pulses, respectively. This is the “conventional” pulse sequence in which one uses a weak probe pulse to investigate the dynamics induced by a strong pump pulse. Additionally, a “counterintuitive” pulse sequence, in which the NIR pulse either overlaps or follows the XUV pulse has been employed in many ATA investigations. Examples of both pulse sequences are given below.

Transient absorption is generally treated in the framework of the third-order polarization in the interaction picture, where an intense pulse (usually the pump) represents a second-order interaction and the weaker pulse (usually the probe) represents a first-order interaction, all in the perturbative limit.^{87,88} More generally, the intense few-cycle near-infrared pulses commonly used in attosecond measurements impart strong fields to the system and require the inclusion of higher-order response functions.^{89,90} The approach to model these experiments is to calculate the single atom response,

$$\tilde{S}(\omega) = -2 \operatorname{Im}[\tilde{d}(\omega)\tilde{E}^*(\omega)]. \quad (2)$$

This approach treats all nonlinearities in one calculation. In eqn (2), $\tilde{d}(\omega)$ is the Fourier transform of the time-dependent one-electron single-atom dipole moment, and the corresponding macroscopic polarization is $\tilde{P}(\omega) = 2\rho\tilde{d}(\omega)$, where ρ is the density of atoms in the interaction region. $\tilde{E}^*(\omega)$ is the Fourier transform of the electric field. The sign of the single-atom response determines whether light is absorbed (positive) or emitted (negative). The absorption cross section is then written as

$$\sigma(\omega) = 8\pi\alpha\omega \operatorname{Im} \left[\frac{\tilde{d}(\omega)}{\tilde{E}(\omega)} \right], \quad (3)$$

where α is the fine-structure constant. Propagation effects through the sample can also be accounted for as necessary.⁹¹

In the conventional pulse ordering for transient absorption, the near-infrared excitation serves as the pump pulse and is followed by the attosecond XUV probe pulse. The XUV spectrum is detected as a function of pump–probe delay. This pulse sequence interrogates population dynamics of the system initiated by the near-infrared pump pulse. It has been used to great effect in femtosecond XUV transient absorption measurements, in which a molecular species such as $\text{C}_2\text{H}_3\text{Br}$ is strong-field ionized by the NIR pump pulse, and the XUV probe pulse comprising harmonics from 60–72 eV monitors core transitions in the Br atoms that are sensitive to its charge state and chemical environment.⁹² One can track the depletion of $\text{C}_2\text{H}_3\text{Br}$, the appearance of $\text{C}_2\text{H}_3\text{Br}^+$ in its X and A electronic states, and the production of Br^+ from dissociative ionization.

In the first attosecond experiment of this type, Kr atoms were strong-field ionized by a NIR pump pulse, ejecting a 4p electron and creating a coherent superposition of the $\text{Kr}^+ 2\text{P}_{1/2}$ and $2\text{P}_{3/2}$ spin–orbit levels.⁹³ A broadband isolated

attosecond pulse probed the set of 4p–3d transitions near 80 eV, and the resulting absorption spectrum was measured as a function of pump–probe delay time. The transitions in this spectral region show clear oscillatory structure with a period of 6.3 fs, corresponding to the energy spacing of 0.67 eV between the two Kr⁺ spin-orbit levels. The underlying theory relating the coherent superposition created by the NIR pulse to the transient absorption signal has also been developed.⁹⁴ This experiment represents a real-time observation of valence-shell electron wave-packet motion, fulfilling one of the primary goals of attosecond science.

This very general method can also be applied to solid samples.⁹⁵ ATA experiments on Si have been carried out according to the scheme shown in Fig. 3.⁹⁶ Here, attosecond pulses tuned to the silicon L_{2,3} band edge near 99 eV are used to follow the dynamics of electrons injected into the conduction band of silicon by few-cycle NIR pulses. The attosecond and NIR pulse durations are less than 100 as and 4 fs, respectively, as characterized by attosecond streaking, and the sample thickness is about 140–250 nm to ensure a reasonable optical density at the L-edge and to minimize group velocity mismatch between the NIR and XUV pulses.

In order to observe more clearly time-dependent effects, it is useful to differentiate the observed ATA spectra, turning band edges into peaks, as shown in Fig. 4. Clearly, many of the peaks in the differentiated spectrum shift and broaden in the presence of the NIR pulse. More detailed analysis shows that some of these effects persist for many hundreds of fs, while others are transient and disappear once the NIR pulse is gone.

The most remarkable result is shown in Fig. 5 (left), where the ATA spectrum at 100.35 eV exhibits a resolved step structure at intervals of 1.3 fs, which is half the period of the NIR driving pulse. This step structure signifies that the electric field, not the pulse envelope, of the NIR pulse is driving population from the valence to conduction band, and that this population transfer occurs *via* a tunneling mechanism, similar to the strong-field induced tunneling to the continuum that forms the basis of HHG in the gas phase.²¹ Fig. 5 (right) presents an intuitive view of this process;⁹⁷ the valence and conduction bands are distorted by the NIR

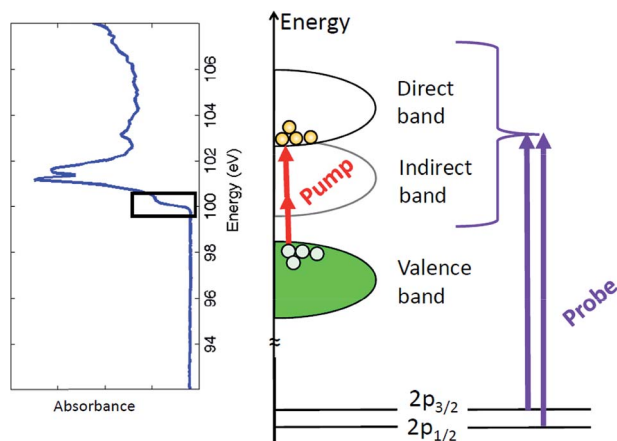


Fig. 3 Principle of ATA experiment in solid Si.

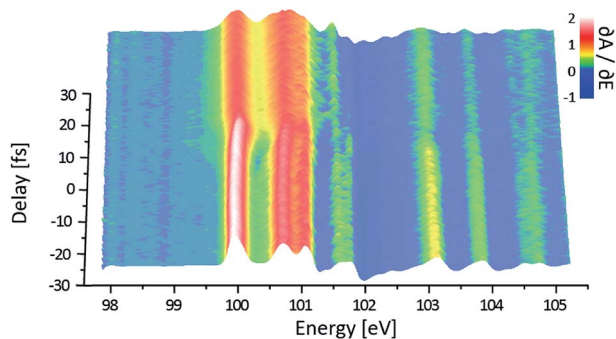


Fig. 4 Derivative of Si ATA spectrum (adapted from ref. 96).

electric field, enabling valence \rightarrow conduction band tunneling near the maxima of the electric field every half period.

A series of gas phase experiments at Berkeley⁹⁸ and elsewhere^{43,44,99–102} have made use of a counterintuitive pulse sequence, in which the XUV pulse overlaps or precedes the NIR pulse. These experiments show that the NIR pulse affects the measured XUV absorption spectrum at delays that are considerably longer than attosecond pulse duration. This effect can be understood with reference to Fig. 6.⁸⁴ If a single transition at energy $E = \hbar\omega_{\text{XUV}}$ is excited by the XUV pulse, the polarization oscillates with frequency ω_{XUV} and exhibits free induction decay (FID) reflecting the lifetime of the excited state. A NIR pulse applied prior to or during the FID can affect the polarization by, for example, ionizing the excited state or coupling it to a manifold of excited states. Taking the Fourier transforms of the polarization signals in Fig. 6 and inserting them into eqn (2) yields the absorption spectra in the right panels of the figure, which clearly show the effect of the NIR pulse. One application of this pulse sequence is the direct

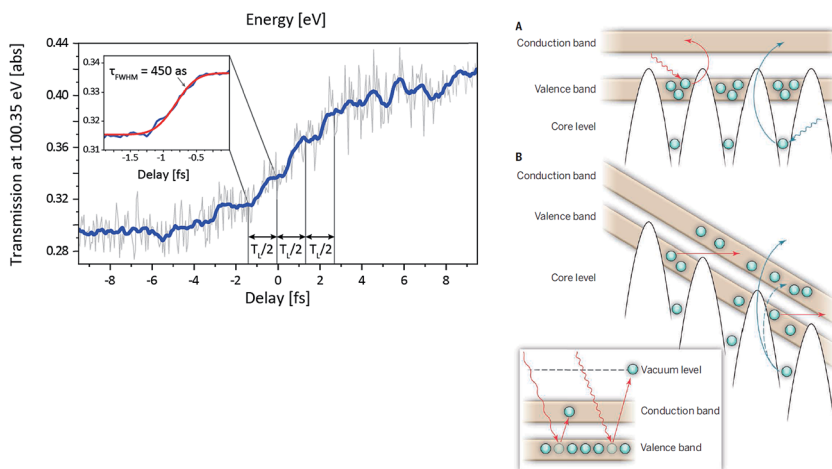


Fig. 5 Sub-cycle step structure in experimental Si spectrum (left) and interpretation in terms of tunneling between valence and conduction bands (right). From references 96 and 97. Reprinted with permission from AAAS.

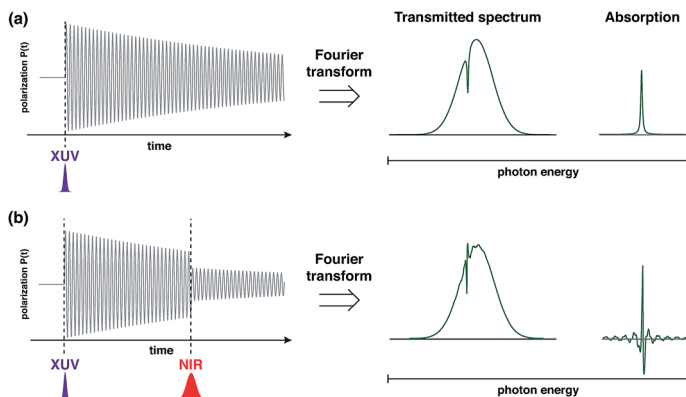


Fig. 6 Principle of ATA experiment with "counterintuitive" pulse sequence. Reprinted from ref. 84 with permission from Elsevier.

measurement of autoionization lifetimes, as demonstrated for Ar and Xe atoms.^{103–105} In one example, illustrated in Fig. 7,¹⁰⁴ an attosecond pulse covering 21–25 eV excites a series of $5s5p^6np$ autoionizing states of Xe. The sharp window resonances corresponding to these transitions are clearly perturbed at short positive delay times, where the NIR pulse arrives after the XUV pulse. Lineouts at the center frequencies of the $n = 6$ and 7 resonances, shown in the right-most panel, exhibit depletion at early times and recovery on time scales of 43.8 and 96.8 fs, respectively. These lifetimes reflect decay times of the excited state wavefunctions owing to autoionization, which are readily shown to be twice the excited state population decay times. Hence, the autoionization lifetimes of the $n = 6$ and 7 states are found to be 21.9 and 48.4 fs, in good agreement with those obtained by linewidth analysis of frequency-domain measurements.

We have also investigated the ATA of Rydberg states of Ar below its ionization potential with a similar pulse sequence.¹⁰⁶ The results are shown in Fig. 8. The XUV pulse promotes a $3p$ valence electron into the Rydberg series $3s^23p^6 \rightarrow 3s^23p^5[{}^2P_{1/2,3/2}]nd(s)$, populating two groups of ns/nd manifolds that converge to different spin-orbit coupled ion core limits, $I_{P[3/2]} = 15.76$ eV and $I_{P[1/2]} = 15.94$ eV. The valence electronic wavepacket initiated by the XUV pulse

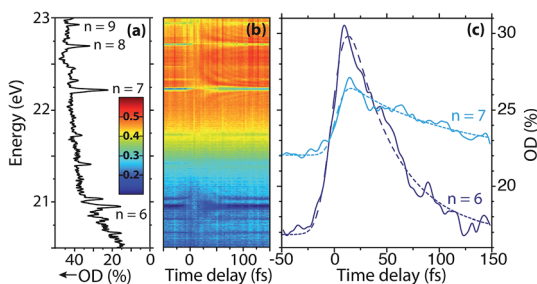


Fig. 7 XUV absorption of Xe (left), ATA spectrum (center), and line-outs showing decay of ATA signals for $n = 6$ and 7 Rydberg states. Reprinted from ref. 104 with permission of the American Physical Society.

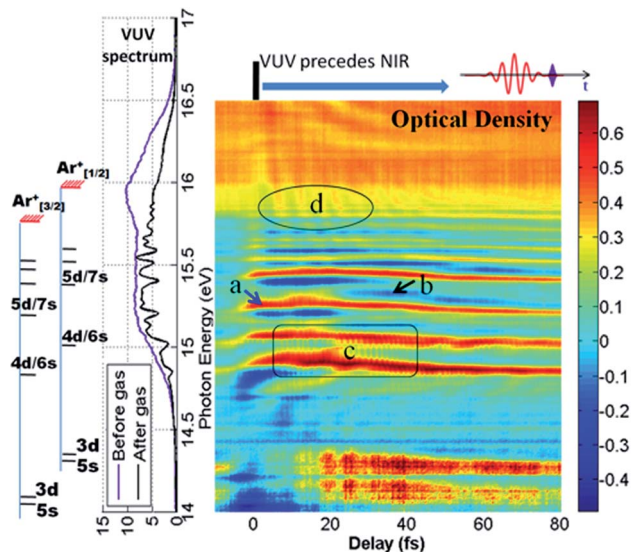


Fig. 8 XUV spectrum of Ar (left) and ATA spectrum (right) from 14–16.5 eV. Reprinted from ref. 106.

experiences an electromagnetic interaction upon the arrival of the NIR pulse. There are four distinct effects attributable to the NIR pulse, each of which is labelled in Fig. 8: (a) broadening and shifting of individual absorption lines at small positive delays, (b) horizontal sideband structures between two adjacent absorption resonances at large positive delays, (c) fast modulations with a period of 1.3 fs on the two 4d states lying around 15 eV, and (d) slow modulations with a period of 5–10 fs on the states approaching the ionization limits (~ 15.75 eV).

Further insight into the oscillatory structures is gained by Fourier analysis of the experimental spectra as shown in Fig. 9, where one can see the relatively slow oscillations near 15.75 eV and the much faster oscillations between 14.75 and 15 eV. The latter are termed “sub-cycle” oscillations since their characteristic period of 1.3 fs is approximately half the period of the NIR field. Likewise, the corresponding energy of 3.2 eV indicated in Fig. 9 corresponds to two NIR photons.

Features (a)–(d) can all be interpreted by means of a simplified many-level nonperturbative treatment that yields the following expression for the $d_1(t)$, the time varying transition dipole between the ground state $|g\rangle$ and excited state $|1\rangle$:

$$d_1(t) \propto e^{-t/t_1} \mu_{1g}^2 \left[|A_1^1(t-\tau)| \sin(E_1 t + \varphi_{A_1^1}) + \sum_{n,n \neq 1} \frac{\mu_{n1g}}{\mu_{1g}} |A_n^1(t-\tau)| \sin(E_1 t + \varphi_{A_n^1} + \Delta E_{n1} \tau) \right] \quad (4)$$

here t_1 is the lifetime of state $|1\rangle$, μ_{n1g} is the dipole matrix element between state $|n\rangle$ and the ground state, τ is the relative time between the XUV and NIR pulses, E_n is the energy of state n , and $\Delta E_{n1} = E_n - E_1$. Atomic units are used throughout. The first term represents NIR laser induced transitions where the initial and final

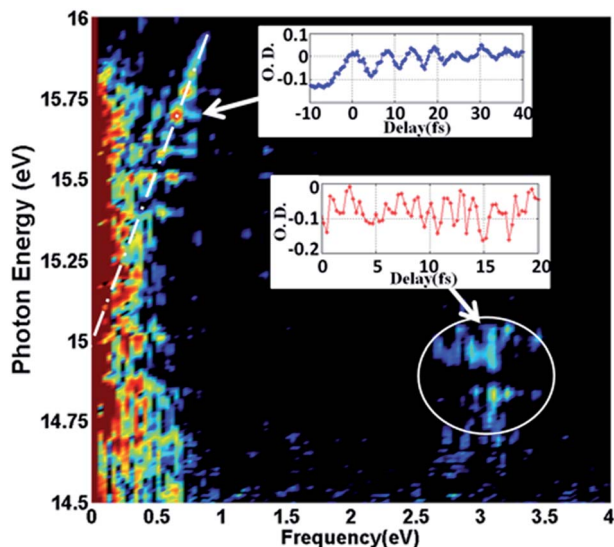


Fig. 9 Fourier analysis of Ar ATA spectrum. Insets show Fourier transform of signals labeled d (upper) and c (lower) in Fig. 8. Reprinted from ref. 106.

states are the same, with $|A_1^1(t - \tau)|$ expressing the laser induced depopulation of state 1 by processes such as ionization and φ_{A_h} the phase corresponding to any energy shift of the state, such as would be caused by the AC Stark effect. The second term describes situations where the final and initial states do not coincide, *i.e.* population transfer processes between states $|1\rangle$ and $|n\rangle$ induced by the NIR pulse. In this case, $|A_n^1(t - \tau)|$ is the magnitude of mutual population transfer and $\Delta E_{n1}\tau$ is the relative phase accumulated by state n during the different time evolution of the two coherently populated states.

Simulations of the spectra using eqn (4) show that features (a) and (b) are due to the AC Stark shift, as they can be reproduced using only the term proportional to $|A_1^1(t - \tau)|$. Feature (a) is a consequence of the impulsive phase shift induced by the short NIR pulse.^{102,107} Feature (b) stems from the interplay between the hyperbolic lines (perturbed free induction decays) originating from two adjacent resonance states¹⁰⁸ and can be used to quantify the AC Stark shift. Features (c) and (d) are due to population transfer involving ladder-type^{43,100,109} and vee-type¹⁰⁸ transition schemes, respectively, as shown in Fig. 10. Essentially, these oscillations reflect interference between two excitation pathways to the same final state: absorption of a single XUV photon, and a three-photon pathway involving absorption of one XUV photon and the interaction with two NIR photons. In ladder-type transitions, the oscillation energy in the Fourier analysis corresponds to the sum of the two NIR photon energies, while in vee-type transitions it corresponds to the difference. The broadband nature of the XUV and NIR pulses make it possible to satisfy the resonance conditions for both types of transitions.

As shown in Fig. 10, the vee and ladder transitions involve the dark Ar $[^2P_{1/2,3/2}]$ 4p Rydberg level as the intermediate state. Moreover, in the Fourier analysis, one can draw a straight line of unity slope through a series of vee-type transitions; the y-intercept yields the energy of one of the states (15 eV, for the white dashed line

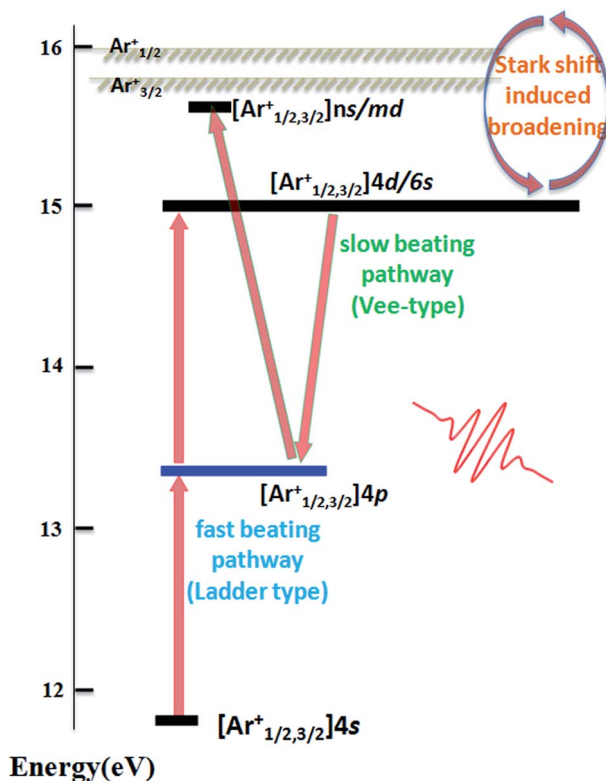


Fig. 10 Origin of interferences between one- and three-photon processes in Ar ATA spectrum.

in Fig. 9) that is coupled *via* the dark state to all the others lying on this line. By the same token, a line of unity slope drawn through the points around 3.2 eV (not shown in Fig. 9) yields the energy of the lower lying state coupled to each upper state by a ladder transition.

Related experiments have recently been reported for electronic states of N_2 near its ionization potential at 15.559 eV.^{86,110} The ATA spectrum of N_2 is complicated by Rydberg series and vibrational progressions lying within this spectral region. Nonetheless, many of the electronic effects seen in rare gas atoms can be discerned in N_2 , in addition to vibrational coherences that are also produced by interference between one- and three-photon processes. Fig. 11 shows results from our laboratory in the region from 12.5–16.7 eV.⁸⁶ The static spectrum in the left panel shows that transitions to the valence b and b' states of N_2 dominate below 15 eV,^{111,112} while the upper energy range is dominated by transitions to Rydberg states converging to the A and B states of N_2^+ .^{113,114}

The density of transitions is clearly higher than in Ar, as expected, but one can still see broadening and shifting of lines, along with sub-cycle and slow oscillations. For example, Fourier analysis of the sub-cycle oscillations shows clusters of states around 15.8 and 13 eV that are coupled by ladder transitions. Schema of the actual electronic states involved are shown in Fig. 12; we believe that the lower

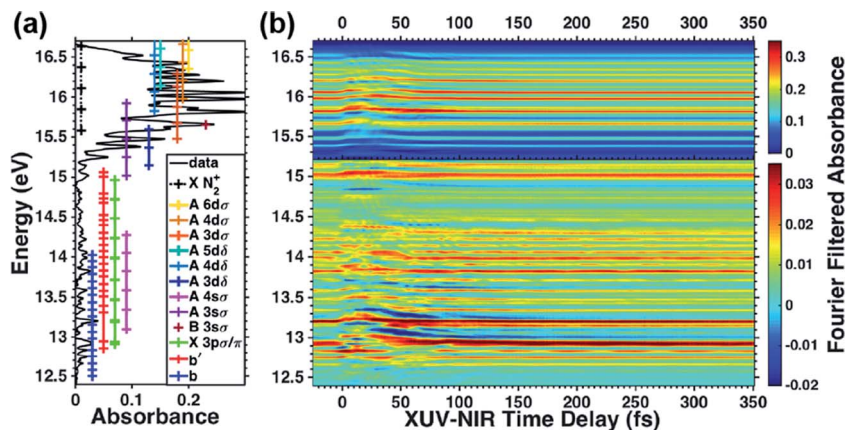


Fig. 11 Static XUV spectrum of N₂ with assignments (left) and ATA spectrum (right). Reprinted from ref. 86 with permission of the American Chemical Society.

and upper states are the b valence state of N₂ and a Rydberg state based on the N₂⁺ A state core, with the dark state being another Rydberg state.

Examination of Fig. 11 around 13 eV shows relatively slow oscillations persisting to 350 fs, the longest delays probed in this experiment. Fig. 13 shows Fourier analysis of this spectral region from 12.4–13.3 eV, starting at a delay time of 100 fs. This procedure excludes the fast dynamics caused by electronic coupling near $t = 0$, and allows us to isolate effects associated with vibrational motion. We indeed observe progressions of evenly spaced peaks in the vertical direction that correspond to the $\nu = 1-8$ levels of the N₂ b state;¹¹¹ the peak spacing of 0.081 eV corresponds to a period of 51 fs. This value matches the vibrational period of the b state and the oscillations are thus attributed to vibrational levels of the b state

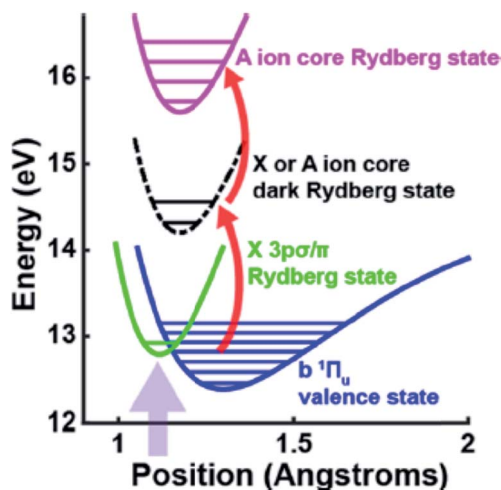


Fig. 12 Schema of electronic states responsible for sub-cycle oscillations in N₂ ATA spectrum near 16 eV. Reprinted from ref. 86 with permission of the American Chemical Society.

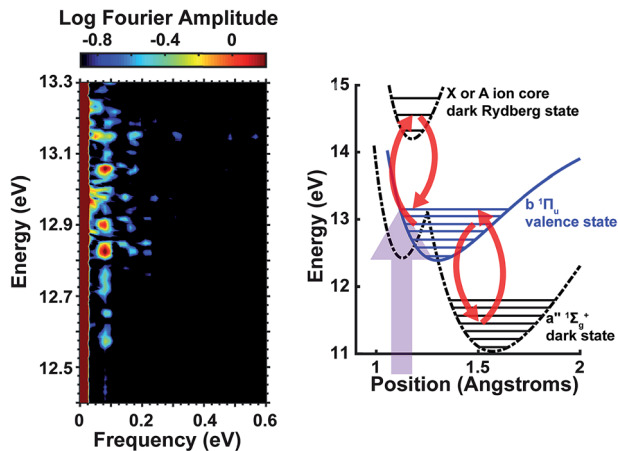


Fig. 13 Fourier analysis of N_2 ATA spectrum from 12.5–14.5 eV, starting at 100 fs in order to emphasize vibrational coherences. Right panel shows possible coupling schemes leading to vibrational coherences. Reprinted from ref. 86 with permission of the American Chemical Society.

separated by $\Delta\nu = \pm 1$ that are coupled by the near IR field. Couplings involving larger values of $\Delta\nu$ can also be seen at some energies. For example, the $\nu = 7$ level at 13.26 eV shows peaks indicating couplings to vibrational levels of the b state down to $\nu = 1$. Overall, these vibrational coherences are attributed to vee-type transitions involving either a higher or lower electronic state as illustrated schematically in Fig. 13.

We close this section by considering two experiments performed on Ne. Fig. 14 shows a section of the transient absorption spectrum of Ne using an isolated attosecond pulse.¹⁰⁸ The two main features in the ATA spectrum at 20.04 eV and 20.14 eV are from transitions to the spin-orbit split ($^2P_{3/2}$)3d and ($^2P_{1/2}$)3d' Rydberg states of Ne. Clear oscillatory structures are seen with a period of 40 fs, which

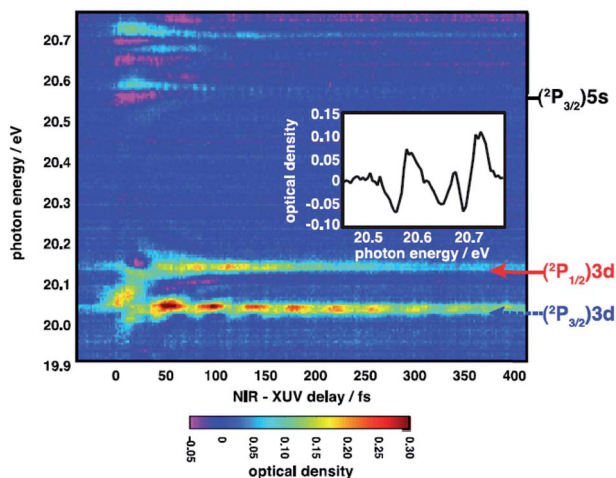


Fig. 14 ATA spectrum of Ne from 19.9–20.8 eV. Reprinted from ref. 108.

corresponds to the spin-orbit splitting of the two Rydberg states. Hence, this beating is attributed to vee-type coupling through an intermediate state, similar to that seen in Ar and N₂.

Recently, we performed a similar experiment on Ne using an attosecond pulse train comprising discrete harmonics in which the 13th harmonic around 20 eV was blocked by an indium filter.¹¹⁵ Fig. 15 shows the dispersed XUV signal with XUV only (black line) and XUV + NIR (red and blue lines). Remarkably, we observe sharp, spatially coherent emission features around 20 eV in the presence of the two pulses. This result can be understood in terms of resonant four-wave mixing (FWM) with reference to Fig. 15. Here, the 11th harmonic at 16.5 eV is resonant with the transition from the ground state to the spin-orbit split (²P_{3/2}, ²P_{1/2})3s state (the 3s and 3s' states). The NIR pulse resonantly couples these upper states to the higher lying 4s/4s' and 3d/3d' levels *via* the intermediate Ne 3p state. The combination of one XUV and two NIR photons induces emission back to the ground state (ω_4 in Fig. 15), resulting in a series of sharp peaks around 20 eV.

These features appear at the same energies as in the ATA spectrum of Ne, but their time-dependence, as shown in Fig. 16, is distinctly different. The oscillation period is 25 fs, corresponding to the energy splitting of 0.17 eV between the 3s and 3s' states. In this experiment, we are thus observing quantum beating between the coherent superposition of states formed by the XUV pulse, rather than interferences between the 3d and 3d' final state by vee-type coupling.

One way to understand the different time-dependences is *via* eqn (5). In this regime, the polarizability $P(\omega)$ is given by

$$P(\omega) = \varepsilon_0\chi^{(1)}E_{\text{XUV}}(\omega) + \varepsilon_0\chi^{(3)}E_{\text{HH}}(\omega_1)E_{\text{NIR}}(\omega_2)E_{\text{XUV}}(\omega_3) \quad (5)$$

The first order term represents linear absorption at ω , and the second term is the third-order contribution to the polarizability. When broadband XUV (and NIR) pulses are used, the frequency condition with $\omega = \omega_1 \pm \omega_2 \pm \omega_3$ is easily satisfied, leading to interference between the first and third order terms; this interference is the origin of much of the time-dependent structure. In contrast, under the experimental conditions of Fig. 15, the first order contribution to the signal around 20 eV is largely absent and the third order term dominates;

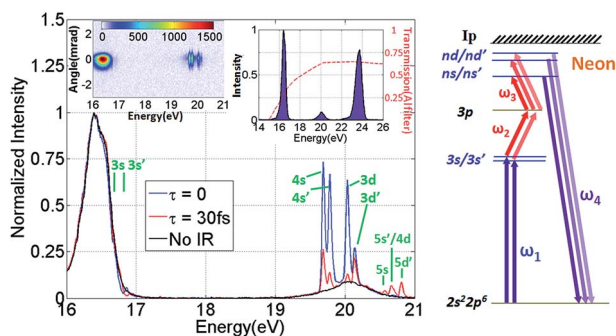


Fig. 15 Left panel shows coherent emission from Ne around 20 eV when pumped by 11th harmonic and two NIR photons. Right panel shows underlying four-wave mixing scheme. Reprinted from ref. 115 with permission of the American Physical Society.

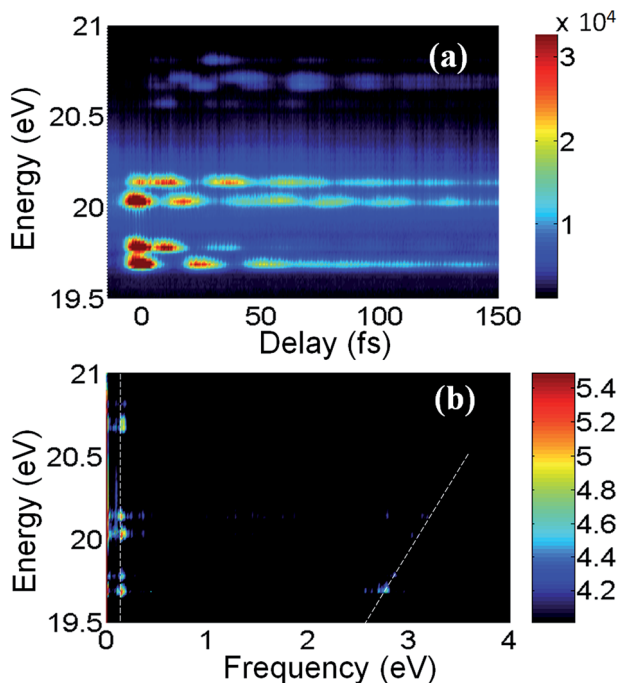


Fig. 16 Time-dependent coherent emission signal from Ne (a) and Fourier analysis of this signal (b). Reprinted from ref. 115 with permission of the American Physical Society.

a description in the language of FWM is more appropriate. We also note that the Ne signals in the FWM configuration (and their Fourier transforms, as shown in the bottom panel of Fig. 16) are considerably simpler than in the ATA experiment. These experiments hint at the potential for carrying out time-resolved non-linear experiments in the XUV, a topic that has received considerable theoretical consideration^{116,117} but little experimental attention up to now.

Outlook and conclusions

Attosecond science is an emerging field with the potential to address fundamental problems of interest in atomic, molecular, and condensed matter physics. While technical challenges in generating attosecond light pulses are still being addressed, it is now possible to apply attosecond methodology to increasingly complex systems and to probe an array of dynamical processes that have previously been inaccessible. In this paper, for example, we have shown how attosecond transient absorption can discern phenomena ranging from field-induced tunneling in solid silicon to time-resolved four-wave mixing in Ne atoms.

In our laboratory, the four-wave mixing experiments described above have recently been extended to a non-collinear geometry,¹¹⁸ allowing one to carry out XUV nonlinear spectroscopy experiments analogous to those in the infrared and visible regions of the spectrum but with sub-fs temporal resolution. The non-adiabatic dynamics of dissociating polyatomic molecules are being investigated with attosecond transient absorption. The broadband probe pulse inherent to

these experiments enables one to follow the chemical shift of a core-electron absorption (*i.e.* the Br atom in CH₃Br) as a molecule dissociates. ATA experiments on VO₂ are providing new information on the earliest stages of the photoinduced insulator-metal transition. We have also carried out attosecond transient reflection experiments on solid Ge samples which are highly complementary to ATA experiments on the same system.

Future advances in attosecond science will involve a combination of technique development and new applications. As the upper limit of accessible photon energies is raised, it becomes possible to follow element-specific dynamics with attosecond time resolution. For example, there is much interest (and some progress) in extending the energy range of isolated attosecond pulses beyond 300 eV,^{33,119} so that one can follow carbon K-edge chemical shifts in real time either by photoemission or transient absorption. Such a development will enable the study of carbon-containing molecules with attosecond methods and will represent a major extension of attosecond science into chemistry. Advanced optical frequency synthesis methods now allow the generation of nearly single-cycle pulses in the visible and ultraviolet region,^{17,120} enabling vis-UV/XUV pump-probe experiments with substantially improved resolution compared to those with few-cycle pump pulses. Accelerator-based light sources will soon be producing attosecond light pulses with significantly higher fluxes and photon energies than laser-based systems, opening up many new directions in attosecond science.

Acknowledgements

This research has been supported by the Director, Office of Science, Office of Basic Energy Sciences, of the US Department of Energy under contract DE-AC02-05CH11231, the Wm. H. Keck Foundation, the Defense Advanced Research Projects Agency PULSE program through grant W31P4Q-13-1-0017, and the Multidisciplinary University Research Initiatives from the Army Research Office (WN911NF-14-1-0383) and the Air Force Office of Scientific Research (FA9550-15-1-0037). S. R. L. acknowledges support from a National Security Science and Engineering Faculty Fellowship (NSSEFF) and from the National Science Foundation under grant CHE-1361226.

References

- 1 A. H. Zewail, *J. Phys. Chem. A*, 2000, **104**, 5660–5694.
- 2 P. B. Corkum and F. Krausz, *Nat. Phys.*, 2007, **3**, 381–387.
- 3 S. R. Leone, C. W. McCurdy, J. Burgdoerfer, L. S. Cederbaum, Z. Chang, N. Dudovich, J. Feist, C. H. Greene, M. Ivanov, R. Kienberger, U. Keller, M. F. Kling, Z. H. Loh, T. Pfeifer, A. N. Pfeiffer, R. Santra, K. Schafer, A. Stolow, U. Thumm and M. J. J. Vrakking, *Nat. Photonics*, 2014, **8**, 162–166.
- 4 K. Zhao, Q. Zhang, M. Chini, Y. Wu, X. W. Wang and Z. H. Chang, *Opt. Lett.*, 2012, **37**, 3891–3893.
- 5 P. Agostini and L. F. DiMauro, *Rep. Prog. Phys.*, 2004, **67**, 813–855.
- 6 M. F. Kling and M. J. J. Vrakking, *Annu. Rev. Phys. Chem.*, 2008, **59**, 463–492.
- 7 T. Pfeifer, M. J. Abel, P. M. Nagel, A. Jullien, Z. H. Loh, M. J. Bell, D. M. Neumark and S. R. Leone, *Chem. Phys. Lett.*, 2008, **463**, 11–24.
- 8 F. Krausz and M. Ivanov, *Rev. Mod. Phys.*, 2009, **81**, 163–234.

- 9 F. Lepine, M. Y. Ivanov and M. J. J. Vrakking, *Nat. Photonics*, 2014, **8**, 195–204.
- 10 L. Gallmann, C. Cirelli and U. Keller, *Annu. Rev. Phys. Chem.*, 2012, **63**, 447–469.
- 11 F. Frank, C. Arrell, T. Witting, W. A. Okell, J. McKenna, J. S. Robinson, C. A. Haworth, D. Austin, H. Teng, I. A. Walmsley, J. P. Marangos and J. W. G. Tisch, *Rev. Sci. Instrum.*, 2012, **83**, 071101.
- 12 M. Chini, K. Zhao and Z. H. Chang, *Nat. Photonics*, 2014, **8**, 178–186.
- 13 F. Krausz and M. I. Stockman, *Nat. Photonics*, 2014, **8**, 205–213.
- 14 K. T. Kim, D. M. Villeneuve and P. B. Corkum, *Nat. Photonics*, 2014, **8**, 187–194.
- 15 F. Calegari, G. Sansone, S. Stagira, C. Vozzi and M. Nisoli, *J. Phys. B: At., Mol. Opt. Phys.*, 2016, **49**, 142001.
- 16 K. Ramasesha, S. R. Leone and D. M. Neumark, *Annu. Rev. Phys. Chem.*, 2016, **67**, 41–63.
- 17 M. T. Hassan, T. T. Luu, A. Moulet, O. Raskazovskaya, P. Zhokhov, M. Garg, N. Karpowicz, A. M. Zheltikov, V. Pervak, F. Krausz and E. Goulielmakis, *Nature*, 2016, **530**, 66–70.
- 18 A. McPherson, G. Gibson, H. Jara, U. Johann, T. S. Luk, I. A. McIntyre, K. Boyer and C. K. Rhodes, *J. Opt. Soc. Am. B*, 1987, **4**, 595–601.
- 19 M. Ferray, A. L. Huillier, X. F. Li, L. A. Lompre, G. Mainfray and C. Manus, *J. Phys. B: At., Mol. Opt. Phys.*, 1988, **21**, L31.
- 20 J. L. Krause, K. J. Schafer and K. C. Kulander, *Phys. Rev. Lett.*, 1992, **68**, 3535–3538.
- 21 P. B. Corkum, *Phys. Rev. Lett.*, 1993, **71**, 1994–1997.
- 22 M. Lewenstein, P. Balcou, M. Y. Ivanov, A. Lhuillier and P. B. Corkum, *Phys. Rev. A*, 1994, **49**, 2117–2132.
- 23 A. Rundquist, C. G. Durfee, Z. H. Chang, C. Herne, S. Backus, M. M. Murnane and H. C. Kapteyn, *Science*, 1998, **280**, 1412–1415.
- 24 M. Bellini, C. Lynga, A. Tozzi, M. B. Gaarde, T. W. Hansch, A. L'Huillier and C. G. Wahlstrom, *Phys. Rev. Lett.*, 1998, **81**, 297–300.
- 25 I. P. Christov, M. M. Murnane and H. C. Kapteyn, *Phys. Rev. Lett.*, 1997, **78**, 1251–1254.
- 26 J. Tate, T. Augustine, H. G. Muller, P. Salieres, P. Agostini and L. F. DiMauro, *Phys. Rev. Lett.*, 2007, **98**, 013901.
- 27 E. J. Takahashi, T. Kanai, K. L. Ishikawa, Y. Nabekawa and K. Midorikawa, *Phys. Rev. Lett.*, 2008, **101**, 253901.
- 28 P. Colosimo, G. Doumy, C. I. Blaga, J. Wheeler, C. Hauri, F. Catoire, J. Tate, R. Chirla, A. M. March, G. G. Paulus, H. G. Muller, P. Agostini and L. F. DiMauro, *Nat. Phys.*, 2008, **4**, 386–389.
- 29 G. Doumy, J. Wheeler, C. Roedig, R. Chirla, P. Agostini and L. F. DiMauro, *Phys. Rev. Lett.*, 2009, **102**, 093002.
- 30 B. E. Schmidt, A. D. Shiner, M. Giguere, P. Lassonde, C. A. Trallero-Herrero, J. C. Kieffer, P. B. Corkum, D. M. Villeneuve and F. Legare, *J. Phys. B: At., Mol. Opt. Phys.*, 2012, **45**, 074008.
- 31 T. Popmintchev, M. C. Chen, D. Popmintchev, P. Arpin, S. Brown, S. Alisauskas, G. Andriukaitis, T. Balciunas, O. D. Mucke, A. Pugzlys, A. Baltuska, B. Shim, S. E. Schrauth, A. Gaeta, C. Hernandez-Garcia, L. Plaja, A. Becker, A. Jaron-Becker, M. M. Murnane and H. C. Kapteyn, *Science*, 2012, **336**, 1287–1291.

- 32 M. C. Chen, C. Mancuso, C. Hernandez-Garcia, F. Dollar, B. Galloway, D. Popmintchev, P. C. Huang, B. Walker, L. Plaja, A. A. Jaron-Becker, A. Becker, M. M. Murnane, H. C. Kapteyn and T. Popmintchev, *Proc. Natl. Acad. Sci. U. S. A.*, 2014, **111**, E2361–E2367.
- 33 F. Silva, S. M. Teichmann, S. L. Cousin, M. Hemmer and J. Biegert, *Nat. Commun.*, 2015, **6**, 6611.
- 34 C. Spielmann, N. H. Burnett, S. Sartania, R. Koppitsch, M. Schnürer, C. Kan, M. Lenzner, P. Wobruschek and F. Krausz, *Science*, 1997, **278**, 661–664.
- 35 D. Popmintchev, C. Hernández-García, F. Dollar, C. Mancuso, J. A. Pérez-Hernández, M.-C. Chen, A. Hankla, X. Gao, B. Shim, A. L. Gaeta, M. Tarazkar, D. A. Romanov, R. J. Levis, J. A. Gaffney, M. Foord, S. B. Libby, A. Jaron-Becker, A. Becker, L. Plaja, M. M. Murnane, H. C. Kapteyn and T. Popmintchev, *Science*, 2015, **350**, 1225–1231.
- 36 N. A. Papadogiannis, B. Witzel, C. Kalpouzos and D. Charalambidis, *Phys. Rev. Lett.*, 1999, **83**, 4289–4292.
- 37 P. M. Paul, E. S. Toma, P. Breger, G. Mullot, F. Auge, P. Balcou, H. G. Muller and P. Agostini, *Science*, 2001, **292**, 1689–1692.
- 38 R. López-Martens, K. Varju, P. Johnsson, J. Mauritsson, Y. Mairesse, P. Salieres, M. B. Gaarde, K. J. Schafer, A. Persson, S. Svanberg, C. G. Wahlstrom and A. L'Huillier, *Phys. Rev. Lett.*, 2005, **94**, 033001.
- 39 Y. Nabekawa, T. Shimizu, T. Okino, K. Furusawa, H. Hasegawa, K. Yamanouchi and K. Midorikawa, *Phys. Rev. Lett.*, 2006, **97**, 153904.
- 40 T. Remetter, P. Johnsson, J. Mauritsson, K. Varju, Y. Ni, F. Lepine, E. Gustafsson, M. Kling, J. Khan, R. Lopez-Martens, K. J. Schafer, M. J. J. Vrakking and A. L'Huillier, *Nat. Phys.*, 2006, **2**, 323–326.
- 41 P. Johnsson, J. Mauritsson, T. Remetter, A. L'Huillier and K. J. Schafer, *Phys. Rev. Lett.*, 2007, **99**, 233001.
- 42 M. Holler, F. Schapper, L. Gallmann and U. Keller, *Phys. Rev. Lett.*, 2011, **106**, 123601.
- 43 M. Lucchini, J. Herrmann, A. Ludwig, R. Locher, M. Sabbar, L. Gallmann and U. Keller, *New J. Phys.*, 2013, **15**, 103010.
- 44 C. Ott, A. Kaldun, L. Argenti, P. Raith, K. Meyer, M. Laux, Y. Z. Zhang, A. Blattermann, S. Hagstotz, T. Ding, R. Heck, J. Madronero, F. Martin and T. Pfeifer, *Nature*, 2014, **516**, 374–381.
- 45 M. Hentschel, R. Kienberger, C. Spielmann, G. A. Reider, N. Milosevic, T. Brabec, P. Corkum, U. Heinzmann, M. Drescher and F. Krausz, *Nature*, 2001, **414**, 509–513.
- 46 E. Goulielmakis, M. Schultze, M. Hofstetter, V. S. Yakovlev, J. Gagnon, M. Uiberacker, A. L. Aquila, E. M. Gullikson, D. T. Attwood, R. Kienberger, F. Krausz and U. Kleineberg, *Science*, 2008, **320**, 1614–1617.
- 47 D. J. Jones, S. A. Diddams, J. K. Ranka, A. Stentz, R. S. Windeler, J. L. Hall and S. T. Cundiff, *Science*, 2000, **288**, 635–639.
- 48 M. Schultze, E. M. Bothschafter, A. Sommer, S. Holzner, W. Schweinberger, M. Fiess, M. Hofstetter, R. Kienberger, V. Apalkov, V. S. Yakovlev, M. I. Stockman and F. Krausz, *Nature*, 2013, **493**, 75–78.
- 49 R. Kienberger, E. Goulielmakis, M. Uiberacker, A. Baltuska, V. Yakovlev, F. Bammer, A. Scrinzi, T. Westerwalbesloh, U. Kleineberg, U. Heinzmann, M. Drescher and F. Krausz, *Nature*, 2004, **427**, 817–821.

- 50 J. Itatani, F. Quere, G. L. Yudin, M. Y. Ivanov, F. Krausz and P. B. Corkum, *Phys. Rev. Lett.*, 2002, **88**, 173903.
- 51 H. Timmers, private communication.
- 52 M. Kovacev, Y. Mairesse, E. Priori, H. Merdji, O. Tcherbakoff, P. Monchicourt, P. Breger, E. Mevel, E. Constant, P. Salieres, B. Carre and P. Agostini, *Eur. Phys. J. D*, 2003, **26**, 79–82.
- 53 G. Sansone, E. Benedetti, F. Calegari, C. Vozzi, L. Avaldi, R. Flammini, L. Poletto, P. Villoresi, C. Altucci, R. Velotta, S. Stagira, S. De Silvestri and M. Nisoli, *Science*, 2006, **314**, 443–446.
- 54 Z. H. Chang, *Phys. Rev. A*, 2007, **76**, 051403.
- 55 H. Mashiko, S. Gilbertson, C. Q. Li, S. D. Khan, M. M. Shakya, E. Moon and Z. H. Chang, *Phys. Rev. Lett.*, 2008, **100**, 103906.
- 56 X. M. Feng, S. Gilbertson, H. Mashiko, H. Wang, S. D. Khan, M. Chini, Y. Wu, K. Zhao and Z. H. Chang, *Phys. Rev. Lett.*, 2009, **103**, 183901.
- 57 T. Pfeifer, A. Jullien, M. J. Abel, P. M. Nagel, L. Gallmann, D. M. Neumark and S. R. Leone, *Opt. Express*, 2007, **15**, 17120–17128.
- 58 A. Jullien, T. Pfeifer, M. J. Abel, P. M. Nagel, M. J. Bell, D. M. Neumark and S. R. Leone, *Appl. Phys. B*, 2008, **93**, 433–442.
- 59 M. J. Abel, T. Pfeifer, P. M. Nagel, W. Boutu, M. J. Bell, C. P. Steiner, D. M. Neumark and S. R. Leone, *Chem. Phys.*, 2009, **366**, 9–14.
- 60 C. A. Haworth, L. E. Chipperfield, J. S. Robinson, P. L. Knight, J. P. Marangos and J. W. G. Tisch, *Nat. Phys.*, 2007, **3**, 52–57.
- 61 K. T. Kim, C. Zhang, T. Ruchon, J.-F. Hergott, T. Auguste, D. M. Villeneuve, P. B. Corkum and F. Quere, *Nat. Photonics*, 2013, **7**, 651–656.
- 62 H. Timmers, M. Sabbar, J. Hellwagner, Y. Kobayashi, D. M. Neumark and S. R. Leone, *Optica*, 2016, **3**, 707–710.
- 63 E. J. Takahashi, P. F. Lan, O. D. Mucke, Y. Nabekawa and K. Midorikawa, *Nat. Commun.*, 2013, **4**, 2691.
- 64 E. Cunningham, Y. Wu and Z. Chang, *Appl. Phys. Lett.*, 2015, **107**, 201108.
- 65 P. Tzallas, E. Skantzakis, L. A. A. Nikolopoulos, G. D. Tsakiris and D. Charalambidis, *Nat. Phys.*, 2011, **7**, 781–784.
- 66 M. Drescher, M. Hentschel, R. Kienberger, M. Uiberacker, V. Yakovlev, A. Scrinzi, T. Westerwalbesloh, U. Kleineberg, U. Heinzmann and F. Krausz, *Nature*, 2002, **419**, 803–807.
- 67 M. Schultze, M. Fiess, N. Karpowicz, J. Gagnon, M. Korbman, M. Hofstetter, S. Neppl, A. L. Cavalieri, Y. Komninos, T. Mercouris, C. A. Nicolaides, R. Pazourek, S. Nagele, J. Feist, J. Burgdorfer, A. M. Azzeer, R. Ernstorfer, R. Kienberger, U. Kleineberg, E. Goulielmakis, F. Krausz and V. S. Yakovlev, *Science*, 2010, **328**, 1658–1662.
- 68 L. R. Moore, M. A. Lysaght, J. S. Parker, H. W. van der Hart and K. T. Taylor, *Phys. Rev. A*, 2011, **84**, 061404.
- 69 J. Feist, O. Zatsarinny, S. Nagele, R. Pazourek, J. Burgdorfer, X. X. Guan, K. Bartschat and B. I. Schneider, *Phys. Rev. A*, 2014, **89**, 033417.
- 70 A. L. Cavalieri, N. Muller, T. Uphues, V. S. Yakovlev, A. Baltuska, B. Horvath, B. Schmidt, L. Blumel, R. Holzwarth, S. Hendel, M. Drescher, U. Kleineberg, P. M. Echenique, R. Kienberger, F. Krausz and U. Heinzmann, *Nature*, 2007, **449**, 1029–1032.
- 71 M. Sabbar, S. Heuser, R. Boge, M. Lucchini, T. Carette, E. Lindroth, L. Gallmann, C. Cirelli and U. Keller, *Phys. Rev. Lett.*, 2015, **115**, 133001.

- 72 M. Uiberacker, T. Uphues, M. Schultze, A. J. Verhoef, V. Yakovlev, M. F. Kling, J. Rauschenberger, N. M. Kabachnik, H. Schroder, M. Lezius, K. L. Kompa, H. G. Muller, M. J. J. Vrakking, S. Hendel, U. Kleineberg, U. Heinzmann, M. Drescher and F. Krausz, *Nature*, 2007, **446**, 627–632.
- 73 G. Sansone, F. Kelkensberg, J. F. Perez-Torres, F. Morales, M. F. Kling, W. Siu, O. Ghafur, P. Johnsson, M. Swoboda, E. Benedetti, F. Ferrari, F. Lepine, J. L. Sanz-Vicario, S. Zherebtsov, I. Znakovskaya, A. L'Huillier, M. Y. Ivanov, M. Nisoli, F. Martin and M. J. J. Vrakking, *Nature*, 2010, **465**, 763–767.
- 74 F. Calegari, D. Ayuso, A. Trabattoni, L. Belshaw, S. De Camillis, S. Anumula, F. Frassetto, L. Poletto, A. Palacios, P. Decleva, J. B. Greenwood, F. Martin and M. Nisoli, *Science*, 2014, **346**, 336–339.
- 75 L. S. Cederbaum and J. Zobeley, *Chem. Phys. Lett.*, 1999, **307**, 205–210.
- 76 A. I. Kuleff, S. Lunnemann and L. S. Cederbaum, *J. Phys. Chem. A*, 2010, **114**, 8676–8679.
- 77 F. Remacle and R. D. Levine, *Proc. Natl. Acad. Sci. U. S. A.*, 2006, **103**, 6793–6798.
- 78 J. Itatani, J. Levesque, D. Zeidler, H. Niikura, H. Pepin, J. C. Kieffer, P. B. Corkum and D. M. Villeneuve, *Nature*, 2004, **432**, 867–871.
- 79 S. Baker, J. S. Robinson, C. A. Haworth, H. Teng, R. A. Smith, C. C. Chirila, M. Lein, J. W. G. Tisch and J. P. Marangos, *Science*, 2006, **312**, 424–427.
- 80 O. Smirnova, Y. Mairesse, S. Patchkovskii, N. Dudovich, D. Villeneuve, P. Corkum and M. Y. Ivanov, *Nature*, 2009, **460**, 972–977.
- 81 S. Haessler, J. Caillat, W. Boutu, C. Giovanetti-Teixeira, T. Ruchon, T. Auguste, Z. Diveki, P. Breger, A. Maquet, B. Carre, R. Taieb and P. Salieres, *Nat. Phys.*, 2010, **6**, 200–206.
- 82 Y. Mairesse, J. Higuette, N. Dudovich, D. Shafir, B. Fabre, E. Mével, E. Constant, S. Patchkovskii, Z. Walters, M. Y. Ivanov and O. Smirnova, *Phys. Rev. Lett.*, 2010, **104**, 213601.
- 83 P. M. Kraus, B. Mignolet, D. Baykusheva, A. Rupenyan, L. Horný, E. F. Penka, G. Grassi, O. I. Tolstikhin, J. Schneider, F. Jensen, L. B. Madsen, A. D. Bandrauk, F. Remacle and H. J. Wörner, *Science*, 2015, **350**, 790–795.
- 84 A. R. Beck, D. M. Neumark and S. R. Leone, *Chem. Phys. Lett.*, 2015, **624**, 119–130.
- 85 L. Gallmann, J. Herrmann, R. Locher, M. Sabbar, A. Ludwig, M. Lucchini and U. Keller, *Mol. Phys.*, 2013, **111**, 2243–2250.
- 86 E. R. Warrick, W. Cao, D. M. Neumark and S. R. Leone, *J. Phys. Chem. A*, 2016, **120**, 3165–3174.
- 87 W. T. Pollard and R. A. Mathies, *Annu. Rev. Phys. Chem.*, 1992, **43**, 497–523.
- 88 S. Mukamel, *Principles of Nonlinear Optical Spectroscopy*, Oxford University Press, New York, 1995.
- 89 M. B. Gaarde, C. Buth, J. L. Tate and K. J. Schafer, *Phys. Rev. A*, 2011, **83**, 013419.
- 90 W. C. Chu and C. D. Lin, *Phys. Rev. A*, 2012, **85**, 013419.
- 91 A. N. Pfeiffer and S. R. Leone, *Phys. Rev. A*, 2012, **85**, 053422.
- 92 M. F. Lin, D. M. Neumark, O. Gessner and S. R. Leone, *J. Chem. Phys.*, 2014, **140**, 064311.
- 93 E. Goulielmakis, Z. H. Loh, A. Wirth, R. Santra, N. Rohringer, V. S. Yakovlev, S. Zherebtsov, T. Pfeifer, A. M. Azzeer, M. F. Kling, S. R. Leone and F. Krausz, *Nature*, 2010, **466**, 739–744.

- 94 R. Santra, V. S. Yakovlev, T. Pfeifer and Z. H. Loh, *Phys. Rev. A*, 2011, **83**, 033405.
- 95 L. J. Borja, M. Zürch, C. D. Pemmaraju, M. Schultze, K. Ramasesha, A. Gandman, J. S. Prell, D. Prendergast, D. M. Neumark and S. R. Leone, *J. Opt. Soc. Am. B*, 2016, **33**, C57–C64.
- 96 M. Schultze, K. Ramasesha, C. D. Pemmaraju, S. A. Sato, D. Whitmore, A. Gandman, J. S. Prell, L. J. Borja, D. Prendergast, K. Yabana, D. M. Neumark and S. R. Leone, *Science*, 2014, **346**, 1348–1352.
- 97 C. Spielmann, *Science*, 2014, **346**, 1293–1294.
- 98 S. H. Chen, M. J. Bell, A. R. Beck, H. Mashiko, M. X. Wu, A. N. Pfeiffer, M. B. Gaarde, D. M. Neumark, S. R. Leone and K. J. Schafer, *Phys. Rev. A*, 2012, **86**, 063408.
- 99 S. Gilbertson, M. Chini, X. M. Feng, S. Khan, Y. Wu and Z. H. Chang, *Phys. Rev. Lett.*, 2010, **105**, 263003.
- 100 X. W. Wang, M. Chini, Y. Cheng, Y. Wu, X. M. Tong and Z. H. Chang, *Phys. Rev. A*, 2013, **87**, 063413.
- 101 F. Martin, Y. Cheng, M. Chini, X. W. Wang, A. Gonzalez-Castrillo, A. Palacios, L. Argenti and Z. H. Chang, in *Xxix International Conference on Photonic, Electronic, and Atomic Collisions*, ed. C. Diaz, I. Rabadan, G. Garcia, L. Mendez and F. Martin, 2015, vol. 635, p. 112070.
- 102 C. Ott, A. Kaldun, P. Raith, K. Meyer, M. Laux, J. Evers, C. H. Keitel, C. H. Greene and T. Pfeifer, *Science*, 2013, **340**, 716–720.
- 103 H. Wang, M. Chini, S. Y. Chen, C. H. Zhang, F. He, Y. Cheng, Y. Wu, U. Thumm and Z. H. Chang, *Phys. Rev. Lett.*, 2010, **105**, 143002.
- 104 B. Bernhardt, A. R. Beck, X. Li, E. R. Warrick, M. J. Bell, D. J. Haxton, C. W. McCurdy, D. M. Neumark and S. R. Leone, *Phys. Rev. A*, 2014, **89**, 023408.
- 105 X. Li, B. Bernhardt, A. R. Beck, E. R. Warrick, A. N. Pfeiffer, M. J. Bell, D. J. Haxton, C. W. McCurdy, D. M. Neumark and S. R. Leone, *J. Phys. B: At., Mol. Opt. Phys.*, 2015, **48**, 125601.
- 106 W. Cao, E. R. Warrick, D. M. Neumark and S. R. Leone, *New J. Phys.*, 2016, **18**, 013041.
- 107 S. Chen, M. Wu, M. B. Gaarde and K. J. Schafer, *Phys. Rev. A*, 2013, **88**, 033409.
- 108 A. R. Beck, B. Bernhardt, E. R. Warrick, M. X. Wu, S. Chen, M. B. Gaarde, K. J. Schafer, D. M. Neumark and S. R. Leone, *New J. Phys.*, 2014, **16**, 113016.
- 109 S. H. Chen, M. Wu, M. B. Gaarde and K. J. Schafer, *Phys. Rev. A*, 2013, **87**, 033408.
- 110 M. Reduzzi, W. C. Chu, C. Feng, A. Dubrouil, J. Hummert, F. Calegari, F. Frassetto, L. Poletto, O. Kornilov, M. Nisoli, C. D. Lin and G. Sansone, *J. Phys. B: At., Mol. Opt. Phys.*, 2016, **49**, 065102.
- 111 P. Gürtler, V. Saile and E. E. Koch, *Chem. Phys. Lett.*, 1977, **48**, 245–250.
- 112 A. Lofthus and P. H. Krupenie, *J. Phys. Chem. Ref. Data*, 1977, **6**, 113–307.
- 113 H. Lefebvre-Brion and K. Yoshino, *J. Mol. Spectrosc.*, 1993, **158**, 140–146.
- 114 H. Lefebvre-Brion, *J. Chem. Phys.*, 2005, **122**, 144315.
- 115 W. Cao, E. R. Warrick, A. Fidler, S. R. Leone and D. M. Neumark, *Phys. Rev. A*, 2016, **94**, 021802.
- 116 I. V. Schweigert and S. Mukamel, *Phys. Rev. Lett.*, 2007, **99**, 163001.
- 117 S. Mukamel, D. Healion, Y. Zhang and J. D. Biggs, *Annu. Rev. Phys. Chem.*, 2013, **64**, 101–127.

Paper

- 118 W. Cao, E. R. Warrick, A. Fidler, D. M. Neumark and S. R. Leone, *Phys. Rev. A*, submitted.
- 119 J. Li, X. Ren, Y. Yin, Y. Cheng, E. Cunningham, Y. Wu and Z. Chang, *Appl. Phys. Lett.*, 2016, **108**, 231102.
- 120 H.-T. Chang, M. Zurch, P. M. Kraus, L. J. Borja, D. M. Neumark and S. R. Leone, *Opt. Lett.*, submitted.